Carbohydrate Polymers 298 (2022) 120024

Contents lists available at ScienceDirect

Carbohydrate Polymers

journal homepage: www.elsevier.com/locate/carbpol

Electron beam treated injectable agarose/alginate beads prepared by electrospraying

Catharina Krömmelbein [a,b,*], Xiaofan Xie [c], Jakob Seifert [b], Robert Konieczny [a], Sabrina Friebe [a,b], Josef Käs [c], Stefanie Riedel [a,b,d,**], Stefan G. Mayr [a,b,*]

[a] Leibniz Institute of Surface Engineering (IOM), Permoserstraße 15, 04318 Leipzig, Germany
[b] Division of Surface Physics, Faculty of Physics and Earth Science, Leipzig University, Linnéstraße 5, 04103 Leipzig, Germany
[c] Soft Matter Physics Division, Peter Debye Institute for Soft Matter Physics, Faculty of Physics and Earth Science, Leipzig University, Linnéstraße 5, 04103 Leipzig, Germany
[d] Cell.Copedia GmbH, Bosestraße 4, 04109 Leipzig, Germany

ARTICLE INFO

Keywords:
High-energy electron irradiation
Injectable hydrogel beads
Shear-thinning and self-healing granular hydrogel

ABSTRACT

Granular hydrogels have evolved into an innovative technology for biomedicine. Unlike conventional hydrogels, granular hydrogels display dynamic properties like injectability and porosity, making them feasible for applications in 3D bioprinting and tissue engineering. High-energy electron irradiation combines sterilization and tuning of hydrogel properties without adding potentially cytotoxic chemicals. In this study, granular agarose/alginate hydrogels are prepared by electrospraying. Utilizing 10 MeV electron irradiation, the granular hydrogels are treated in a dose range of 0 kGy–30 kGy relevant for sterilization. Herein, a size reduction of the microparticles is observed. Mechanical properties of individual agarose/alginate beads are examined using AFM measurements revealing a gel softening attributed to radiation induced chain scission. Shear-thinning and self-healing characteristics of the entire granular hydrogel are studied employing rheology. Although viscoelasticity changes under irradiation, shear-thinning and self-healing prevails. These dynamic properties enable injection, which is demonstrated for 27 G needles. This study presents a mechanical characterization of high-energy electron irradiated granular agarose/alginate hydrogels that extends the diversity of available injectable hydrogels and provides a basis for biomedical applications of this scaffold.

1. Introduction

Common hydrogels are highly hydrated materials formed by complex polymeric networks. So far, hydrogels are used in a wide range of biomedical applications including drug delivery and tissue repair strategies (Aswathy, Narendrakumar, & Manjubala, 2020). However, conventional hydrogels cannot always adequately satisfy the complex requirements stemming, for example, from the structural heterogeneity of human tissue. Moreover, conventional hydrogels often possess pores in the nanoscale-range which impairs cell spreading and migration. Various strategies have been developed to overcome nanoporosity, including freeze-drying or using foaming agents and porogens (De France, Xu, & Hoare, 2018). However, these complex methods involve multiple steps and additives that may not be cytocompatible, which is disadvantageous for many applications.

In the last years, granular hydrogels emerged as a versatile and powerful platform to meet the complex demands. Granular hydrogels consist of accumulated hydrogel particles with micrometer size, referred to as beads. Compared to colloidal suspensions, granular hydrogels have a larger particle size (above 10 μm), that is accompanied with a decreased influence of thermal motion and a greater influence of friction (Riley, Schirmer, & Segura, 2019). A reduction of the dispersion medium can turn the beads from free-floating, unjammed into a jammed state. In the jammed state they exhibit unique physical properties like self-assembly, shear-thinning and self-healing (Daly, Riley, Segura, & Burdick, 2019). Due to this functional and dynamic nature, they are ideal candidates for applications in three dimensional (3D) bioprinting or surgical injections, where they serve as scaffolds for cell migration (Cheng, Zhang, Liu, & Yu, 2020). Moreover, the utilization of granular hydrogels as microcarriers for cell culture (Chen et al., 2020), tissue

* Corresponding authors at: Leibniz Institute of Surface Engineering (IOM), Permoserstraße 15, 04318 Leipzig, Germany.
** Correspondence to: S. Riedel, Cell.Copedia GmbH, Bosestraße 4, 04109 Leipzig, Germany.
E-mail addresses: catharina.kroemmelbein@iom-leipzig.de (C. Krömmelbein), stefanie.riedel@iom-leipzig.de (S. Riedel), stefan.mayr@iom-leipzig.de (S.G. Mayr).

https://doi.org/10.1016/j.carbpol.2022.120024
Received 10 June 2022; Received in revised form 16 August 2022; Accepted 21 August 2022
Available online 8 September 2022

repair (Qazi & Burdick, 2021) or the usage in drug delivery systems (Chen, Shi, Liu, Li, & Cao, 2021) indicates the high versatility of granular hydrogels.

For these purposes, agarose and alginate are interesting candidates. In the past, they have gained increasing attention due to their high biocompatibility and adjustable mechanical properties, which allow for high applicability. They are widely accepted biomaterials in the fields of e. g. drug release, wound healing or tissue engineering (Alizadeh et al., 2019; Guastaferro, Reverchon, & Baldino, 2021; Zeng, Han, Li, & Chang, 2015). So far, agarose and alginate beads have been already employed as supporting bath in 3D bioprinting applications (Jeon et al., 2019; Moxon et al., 2017), as drugs release agents (Khodadadi Yazdi et al., 2020) and in affinity chromatography strategies (An et al., 2020). In addition, Orive et al. (2001) demonstrated the inhibition of tumor angiogenesis by immobilizing VE–cadherin-secreting hybridoma cells in alginate-–agarose microcapsules. This study shows that microencapsulated cells can be employed as a drug delivery system and excellently demonstrates the applicability of agarose/alginate-based beads. Usually, alginate beads are prepared via the dropping-method providing beads in the millimeter order (Kim et al., 2021). Herein, the electrospray technique is used to obtain beads with smaller diameter. Electrospraying and its relative electrospinning are advantageous methods that enable the fabrication of electrosprayed particles even in core-shell or Janus design (Liu et al., 2021), electrospun nanofibers (He et al., 2022) or beads-on-a-string products (Li, Wang, Song, Yu, & Bligh, 2021), a combination of both. Both methods belong to the electrohydrodynamic atomization (EHDA) processes. EHDA describes the ejection of fine jets or/and droplets from a capillary by applying an external electric field due to the interactions between the electrostatic energy and the solution (He et al., 2022). The formation of fine charged droplets arises due to Coulomb repulsion breaking the bulk solution's surface (Hartman, Brunner, Camelot, Marijnissen, & Scarlett, 2000). In this way, droplets are emitted through a needle and subsequently collected. In case of producing alginate beads, a low concentrated calcium chloride ($CaCl_2$) solution often serves as gelling agent (Kim et al., 2021).

For biomedical use, sterilization is required. Electron irradiation is an accepted sterilization method in biology and medicine and known to tune hydrogels in a non-toxic way without requiring supplementary reagents (Ighigeanu et al., 2006). Since electron beams facilitate high dose rates, this technique is advantageous with respect to γ-radiation. In addition, it offers a greater penetration depth compared to ultraviolet-radiation (Ashfaq et al., 2020). However, the exposure of polymeric materials to ionizing irradiation leads to two different processes. First, cleavage or degradation of the polymer may occur, causing a reduction in molecular weight (von Sonntag, 1980). And second, crosslinking mechanisms can lead to a raising molecular weight by the introduction and recombination of covalent bonds (Hennink & van Nostrum, 2012). In terms of mechanical behavior, the impact of irradiation can result in either improved or reduced properties. Aim of this study was to evaluate the mechanical properties of electron beam treated granular agarose/alginate hydrogels using doses up to 30 kGy in contrast to un-irradiated. This study demonstrates further, that granular agarose/alginate hydrogels can be sufficiently densified into an injectable scaffold. Herein, we provide a fundamental basis for applications of this scaffold in the fields of tissue engineering or improved drug delivery. Electron irradiation may paves a way to tailor the material properties of the presented scaffold for better functional applications.

2. Experiment

2.1. Agarose/alginate hydrogel preparation

Alginic acid sodium salt was purchased from Thermo Fisher Scientific (Cat. No.: 177772500, Germany). According to the supplier it has a viscosity of 350 mPa s–550 mPa s at a concentration of 1 wt% and a temperature of 20 °C. Guluronic acid content is ~60 %. Preweighed amounts of alginic acid sodium salt were dissolved in dH_2O to obtain a 1 wt% solution. The sodium alginate solution was stirred at room temperature for 2 h and heated to 40 °C.

Meanwhile an agarose solution was prepared. Agarose (Carl Roth GmbH+ Co. KG, Cat. No.: 6351.1, Germany) with a sol-gel-transition and gel-sol-transition temperature of 28 °C and 65.5 °C, respectively, was used. Gel strength corresponds to $\leq$500 g cm^{-2} at a concentration of 1.5 wt%. According to the manufacturer, the water and sulfate contents were less than 10 % and 0.12 %, respectively. Agarose was dissolved in dH_2O to form a 1 wt% solution and boiled in a water bath for 20 min.

The agarose/alginate solution was mixed in a 6/4 ratio. For a homogeneous mixture, the solution was stirred at 40 °C for 15 min.

2.2. Electrospraying

Agarose/alginate beads were fabricated using an electrospray device (Spraybase, 30 kV Electrospinning and Electrospraying Kit, Ireland). To prevent gelation, the solution was sprayed at an ambient temperature of 35 °C and a humidity of 50 %.

The solution was transferred to a 30 G capillary by a syringe pump with a flow rate of 50 µl min^{-1}. Between the capillary and the collecting bowl, a voltage of 5 kV, 10 kV or 15 kV was applied. A 0.2 mol l^{-1} $CaCl_2$ solution was employed to collect the agarose/alginate beads. $CaCl_2$ was purchased by Thermo Fisher Scientific (Cat. No.: L13191.30, Germany) and dissolved in dH_2O. The $CaCl_2$ solution was stirred during electrospraying to prevent agglomeration.

Thereafter, the beads were stored at 6 °C for 24 h. Then, they were washed three times with dH_2O to remove the residual $CaCl_2$. Next, they are irradiated by high-energy electrons. Between measurements, the beads were stored in water at a temperature of 6 °C.

2.3. High-energy electron irradiation

For high-energy electron irradiation, a 10 MeV electron accelerator (MB10-30MP; Mevex Corp., Canada) was employed. The accelerator is equipped with a moving stage with maximum speed of 3 m min^{-1}. The samples were scanned with a frequency of 3 Hz by the scanning horn. The pulsed electron beam had a length and repetition rate of 8 µs and 180 Hz, respectively. The desired irradiation doses were achieved by intervals of 5 kGy (Wisotzki et al., 2014). For dose detection, a graphite dosimeter with error of about 10 % was utilized. The samples were irradiated in dH_2O and cooled to room temperature by draft to reduce heating during irradiation.

2.4. Bead size analysis

A confocal microscope (IX71, Olympus Life Science, Germany) was used to record images of the beads suspended in dH_2O. The images were edited using ImageJ (Schneider, Rasband, & Eliceiri, 2012). The radius of the spheres was determined with a self-written Matlab script based on circular Hough transformation (Hough, 1962). The polydispersity index *PDI* of the beads was calculated as follows; $PDI = \left(\frac{\sigma}{d}\right)^2$ where σ denotes the standard deviation and d the diameter of the beads. For statistical analysis, a normality test and a Mann-Whitney U test was examined with $p < 0.05$.

2.4.1. Voltage variation

The electrospray voltage was set to 5 kV, 10 kV and 15 kV while the electrospray flow rate and the electron dose was kept constant at 50 µl min^{-1} and 0 kGy, respectively. For each voltage, the diameter of the beads were determined. This experiment was repeated three times independently to ensure statistical relevance. For each experiment, 30 images were taken. Thus, a minimum of 90 images and 6442 beads per voltage was measured.

2.4.2. Electron dose variation

In all irradiation doses (0 kGy, 10 kGy, 20 kGy and 30 kGy), the beads were prepared at constant electrospray parameters in three independent fabrication processes. In each fabrication process, the electrospray voltage and flow rate was 15 kV and 50 µm min^{-1}, respectively. The three fabrication processes were irradiated in three independent treatments. For each fabrication process, 30 images were acquired. Thus, 90 images and at least 6588 beads were measured per electron dose.

2.5. Rheology

A MCR-300 bulk rheometer (Anton Paar, Austria) in rotational oscillation was utilized to study the global granular hydrogel. The investigated granular hydrogel was prepared using a voltage of 5 kV and a flow rate of 50 µm min^{-1}. 150 µl of the bead solution was measured with a gap of 0.3 mm via parallel plate geometry. The probe head had a diameter of 25 mm. Prior, excess water of the bead solution was removed by centrifugation. Each measurement was performed at a temperature of 25 °C. First, cyclic measurements were carried out by cycling between 0.1 % and 1000 % strain γ at a frequency of 1 Hz. Then, a γ sweep ranging from 0.1 % to 1000 % at 1 Hz was performed with the same sample. Finally, oscillatory frequency sweeps were conducted from 0.1 Hz to 10 Hz at $\gamma = 0.1$ %. At least nine experiments were performed per irradiation dose, i.e. three per manufacturing process for three independent manufacturing processes.

2.6. AFM

Microrheology of individual beads was investigated using an atomic force microscope (NanoWizard 4 XP NanoScience, JPK BioAFM — Bruker Nano GmbH, Germany). It is equipped with a hybrid stage and an Axio Zoom.V16 microscope (Carl Zeiss AG, Germany). The microscope is guided by a NanoWizard V7 software (JPK BioAFM — Bruker Nano GmbH, Germany). An individual bead was indented with a tipless cantilever (TL-FM Nanosensors, 28 µm ± 7.5 µm cantilever width, NanoWorld AG, Switzerland). Nominal spring constant of the cantilever was $k = 2.8$ N m^{-1}. The indentation force was 100 nN for each measurement. A sinusoidal oscillation with frequency of 1 Hz, 3 Hz, 10 Hz, 30 Hz, 100 Hz and 200 Hz was applied. The oscillation amplitude was 15 nm. At least two independent manufacturing processes of the beads were investigated per irradiation dose. 10 beads were measured per process and each bead was measured three times, resulting in a minimum of 60 measurements. Electrospray parameter of the investigated beads were 5 kV and 50 µm min^{-1}.

The force F-indentation δ curves were analyzed by a Hertz fit using JPK software. Prior, the curves were smoothed and baseline corrected. Applying Hertz model (Hertz, 1882) permits the calculation of the elastic Young's modulus E according to previous studies (Mahaffy, Shih, MacKintosh, & Käs, 2000):

$$F = \frac{4}{3}\frac{E}{1-\nu^2}\sqrt{R\delta^3} \Leftrightarrow E = \frac{3}{4}\frac{F(1-\nu^2)}{\sqrt{R\delta^3}}. \quad (1)$$

where ν denotes the Poisson's ratio taken as $\nu = 0.5$, while R corresponds to the radius of the bead. The projected area is considered to be a circular contact area with a diameter equivalent to the width of the cantilever. However, to describe viscoelastic materials using the Hertz model, frequency-dependent behavior needs to be taken into account. Eq. 1 can thus be extended by the Taylor series (Mahaffy et al., 2000):

$$E = \frac{(1-\nu^2)}{2\sqrt{R\delta_0}}\frac{F(\omega)}{\delta(\omega)} \quad (2)$$

with δ_0 describing the mean indentation. The angular frequency ω dependent force $F(\omega)$ and indentation $\delta(\omega)$ is expressed as follows: $F(\omega) = F_A \cdot \exp(i\phi_F)$ and $\delta(\omega) = \delta_A \cdot \exp(i\phi_\delta)$, respectively. Since the phase shift $\Delta\phi$ between force and indentation corresponds to $\Delta\phi = \phi_F - \phi_\delta$, $F(\omega)$ and $\delta(\omega)$ result in: $F(\omega) = F_A \cdot \exp(i\Delta\phi)$ and $\delta(\omega) = \delta_A$ (Alcaraz et al., 2003). Now Eq. 2 can be written as:

$$E = \frac{(1-\nu^2)}{2\sqrt{R\delta_0}}\frac{F_A}{\delta_A}\cdot exp(i\Delta\phi). \quad (3)$$

Euler's formula and the shear modulus expression $G = E/(2(1+\nu))$ correlate Young's modulus and storage G' and loss moduli G'' (Landau & Lifshitz, 1959). This finally leads to:

$$G^*(\omega) = G'(\omega) + iG''(\omega) = \frac{1-\nu}{4\sqrt{R\delta_0}}\frac{F_A}{\delta_A}\cdot(cos(\Delta\phi) + isin(\Delta\phi)). \quad (4)$$

3. Results and discussion

3.1. Bead size analysis: impact of voltage variation

In this study, 1 wt% agarose/alginate beads (ratio 6/4) were prepared by electrospraying and modified using high-energy electron irradiation. First, different electrospray voltages are investigated at a dose of 0 kGy while electrospray flow rate is kept constant at 50 µl min^{-1}. Fig. 1 shows the size distribution of agarose/alginate beads in dependence on the applied voltage during electrospraying. With increasing voltage, the bead size decreases with radii ranging from 60.0 µm ± 15.3 µm at 5 kV to 40.9 µm ± 8.2 µm at 15 kV. All voltages are in jet flow regime instead of electrostatic dripping mode as they produce beads smaller than the diameter of the electrospray needle. Once in the jet mode, it is frequently reported, that the particle size decreases with increasing voltage, attributed to the greater acceleration of the beam current (Zakeri, Moghadam, Samimi, & Mohebbi-Kalhori, 2019). In contrast to most other studies, we observe a relatively high polydispersity with an index *PDI* of 0.06 at 5 kV and 0.05 at 15 kV. The high polydispersity can be assigned to the mix of the two polymers agarose and alginate, as the polymer's molecular weight and type is known to affect the size and shape of the electrosprayed beads (Wu & Clark, 2007). While the shape of our beads is roughly spherical, see representative images in Fig. 2, the size distribution is broader when compared to another study spraying pure alginate (Park et al., 2012). A higher polydispersity with semi bimodal bead size distribution is reported in the literature (Jafari-Nodoushan, Barzin, & Mobedi, 2015). These authors investigated electrospraying of polylactic-co-glycolic acid (PLGA) with different ratios of lactic acid to glycolic acid, resulting in a similar polydispersity.

Higher proportions of agarose in the hydrogel still lead to gelation in

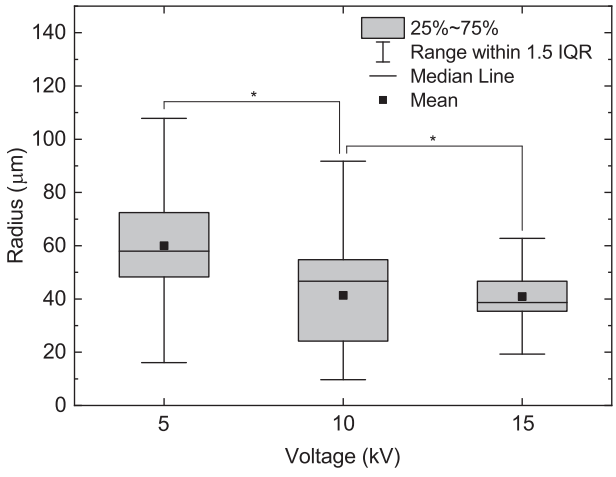

Fig. 1. Dependence of the size distribution of 1 wt% agarose/alginate beads on the applied electrospray voltage. Electron dose is 0 kGy for all measurements. Asterisks indicate statistical significance ($p < 0.05$).

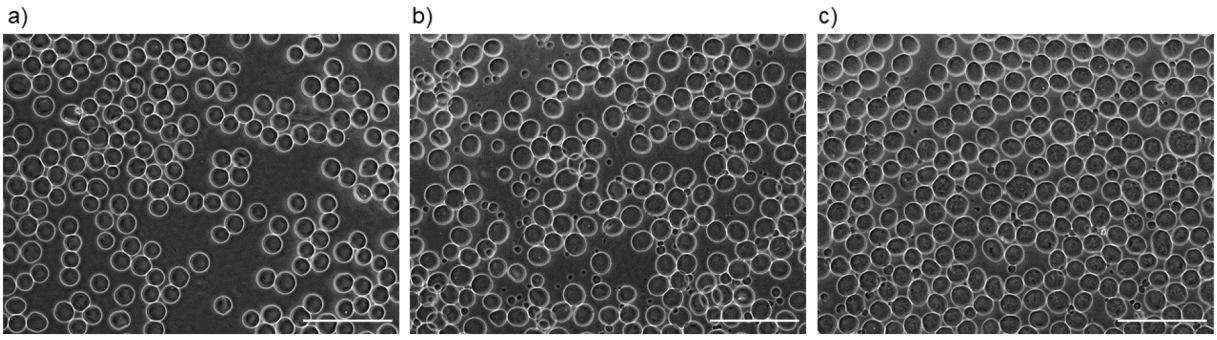

Fig. 2. Representative phase-contrast images of 1 wt% agarose/alginate beads prepared by electrospray voltages of 5 kV (Fig. 2a), 10 kV (Fig. 2b) and 15 kV (Fig. 2c). Electron dose was 0 kGy. Scale bar indicates 500 μm.

the $CaCl_2$ bath, but also to a less spherical droplet shape (see Fig. S1 in supplementary material). This might be assigned to an increased polymerization time and a slower conservation of the spherical form. However, when comparing our produced agarose/alginate beads with those of pure alginate at the same parameters from other studies (Park et al., 2012; Vicini, Castellano, Mauri, & Marsano, 2015), our beads appear slightly smaller. This effect might be due to the lower viscosity of the agarose solution, compared to alginate. A higher viscosity is thought to increase the resistance of the solution to form droplets and results in larger beads (Hartman et al., 2000). According to the theory introduced by Rosell-Llompart & Fernández de la Mora, 1994, the solution's viscosity plays a major role in the liquid jet breakup and consequently affects the bead size. Smaller radii of the beads could have been achieved using lower flow rates (de la Mora & Loscertales, 1994; Park et al., 2012), since the flow rate Q is directly proportional to the particle diameter $d \propto Q^{1/3}$. However, a reduced flow rate is accompanied by a decreased particle yield. Higher voltages did not lead to the formation of beads, but to a thin film on the surface of the collecting $CaCl_2$ solution (not shown here). To avoid this, the surface tension of the $CaCl_2$ solution would have to be reduced. This would probably result in smaller radii, but would also reduce the biocompatibility of the beads.

3.2. Bead size analysis: impact of electron dose

Agarose/alginate beads are fabricated using electrospray and subsequently modified by 10 MeV electron irradiation. To investigate the sterilization relevant dose range, electron doses of 0 kGy, 10 kGy, 20 kGy and 30 kGy are applied. After irradiation, the radii of the beads are detected. In Fig. 3, the size distribution of the agarose/alginate beads is shown in dependence on electron dose. Representative phase-contrast images after electron irradiation with 10 kGy, 20 kGy and 30 kGy are found in Fig. 4. The investigated beads are prepared using a voltage of 15 kV. The size analysis shows a size reduction of ~20% from 40.9 μm at 0 kGy to 32.5 μm at 30 kGy. This indicates a degradation which is already reported in refs. von Sonntag (1980) and Wang et al. (2015). Under high-energy electron irradiation, $OH^{\bullet}$ and $H^{\bullet}$ radicals form by hydrolysis which can react with the carbohydrates. The water radicals are able to abstract hydrogen atoms from the carbohydrates resulting in macroradicals. The macroradicals further react, leading to polymer chain scission or inter- and intramolecular recombination known as crosslinking. Since agarose and alginate is reported to be degradable under ionizing irradiation (Wang et al., 2015; Wasikiewicz, Yoshii, Nagasawa, Wach, & Mitomo, 2005) we assume that polymer chain cleavage is the dominating mechanism when irradiating our agarose/alginate beads. The scission of the glycosidic bond leads to the reduction of the molecular weight (Nagasawa, Mitomo, Yoshii, & Kume, 2000; Wang et al., 2015) which results in carbonyl containing species. Thus, we conclude that the cleavage of carbohydrates by electron irradiation leads to the reduction of the bead size. This assumption is supported by the formation of small agarose/alginate species after electron beam treatment, visualized in Fig. 5. The species have a size of approx. 3 μm–5 μm. They can be easily washed away and did not affect our bead size analysis. In addition, the amount of the species increase with increasing electron dose. Their formation might be supported by the effect of polymer chain scission, and at the same time lead to the size reduction of the beads, due to the increased pressure in spheres by the impact of surface tension (Young-Laplace equation). In this dose range, neither a liquefying nor the formation of gas cavities in the beads is observed as reported for γ- and electron irradiated agarose (Krömmelbein et al., 2021; Wang et al., 2015). The omission of gas cavities might be explained by smaller diffusion paths in the microbeads compared to macroscopic hydrogels, allowing the gas to diffuse out faster.

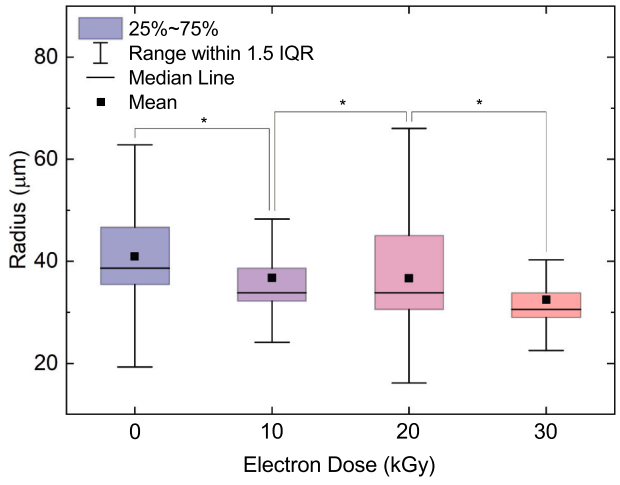

Fig. 3. Size distribution of 1 wt% agarose/alginate beads in dependence on electron dose. Asterisks represent statistical significance ($p < 0.05$).

3.3. Rheology

While most studies focus on collodial suspensions with rigid particles, the mechanics of non-Brownian, viscoelastic particles is less well investigated (Gilbert, Valette, & Lemaire, 2022). Interestingly, granular hydrogels are advantageous in widespread biomedical applications ranging from drug delivery to tissue engineering (Daly et al., 2019). Hence, we simulated the conditions of injection, crucial for many applications, by rotational oscillation rheometer measurements. Herein, the mechanics of the global granular hydrogel irradiated with 0 kGy–30 kGy was investigated. The granular hydrogel was manufactured using an electrospray voltage of 5 kV. The samples undergo multiple cycles of high (1000 %) and low strain (0.1 %) at constant frequency of 1 Hz. Storage G' and loss moduli G'' are shown in Fig. 6. In the low strain γ regions, the granular hydrogels maintained relatively high mechanics with $G' \approx 504$ Pa for un-irradiated samples and slightly stiffen with time.

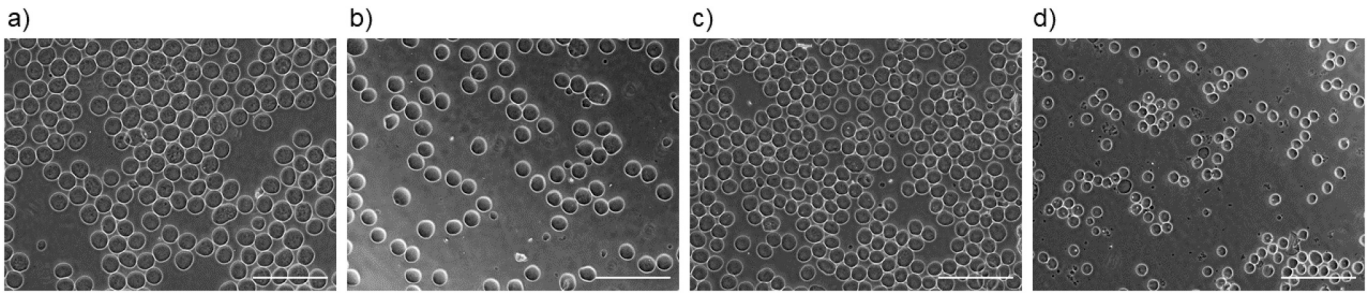

Fig. 4. Representative phase-contrast images of 1 wt% agarose/alginate beads with irradiation doses of 0 kGy (a), 10 kGy (b), 20 kGy (c) and 30 kGy (d). For all images, electrospray voltage is 15 kV. Scale bars indicate 500 μm.

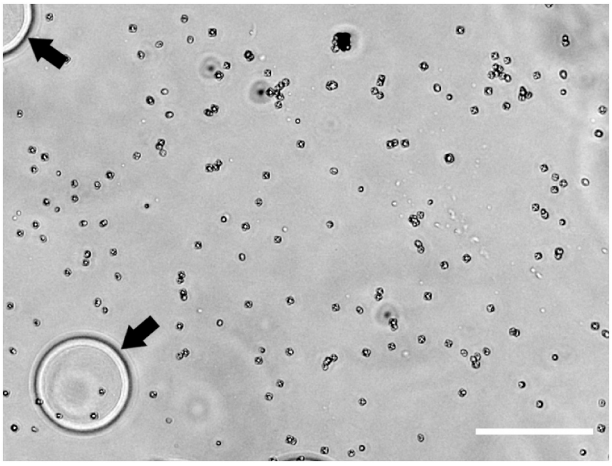

Fig. 5. Phase-contrast image of 1 wt% agarose/alginate beads (indicated by black arrows) irradiated with 20 kGy to visualize the formation of significantly smaller separated species. Voltage is 5 kV, scale bar represents 100 μm.

In high strain γ regions, the samples adopted liquid-like ($G' \approx 2$ Pa) within the next measurable point (approx. 16 s). After applying high strain γ, the moduli recovered the initial values of solid-like behavior in the low strain γ regions, which is indicated by $G' > G''$ (dissipation factor: $\tan\delta < 1$). Thus, the granular hydrogels exhibit shear-thinning and self-healing behavior (Riley et al., 2019), characterized by viscous flow under shear stress and recovery after stress removal, respectively. This allows maintained viscoelastic properties after injection, without further chemical modification, secondary inter-particle crosslinking or waiting for polymerization. For each dose, recovery after applying 1000 % strain takes approx. 44 s, almost three times longer as the first measurable point after conversion into liquid-like behavior. Thus, recovery kinetics are remarkably slow which might be assigned to reassembling of the beads to recover from layering in high-strain regions. Furthermore, G' and G'' are significantly smaller than bulk agarose hydrogels (Krömmelbein et al., 2021). Here, about 13000 Pa and 1500 Pa were reported for G' and G'' at 0 kGy, respectively. Our significantly smaller values may result due to the bead's mobility and interstitial spaces. However, our storage moduli are still within the range of recently published granular hydrogels out of modified hyaluronic acid (Muir, Qazi, Shan, Groll, & Burdick, 2021) or oxidized and methacrylated alginate (Jeon et al., 2019). While the self-healing behavior of our granular hydrogels is clearly observable by the cyclic strain γ measurements shown in Fig. 6, we additionally demonstrate shear-thinning by conducting strain sweeps shown in Fig. 7. Herein, the viscosity η is plotted as a function of shear rate $\dot{\gamma}$. The shear-thinning i. e. pseudoplasticity is represented by the linear decrease of η with increasing $\dot{\gamma}$. The linear region can be expressed by the Ostwald-de Waele relationship (Ostwald, 1925): $\eta = k\dot{\gamma}^{(n-1)}$. k and n corresponds to the flow consistency and flow behavior index, respectively. k is 12.42 Pa s^n, 6.41 Pa s^n, 3.06 Pa s^n and 1.91 Pa s^n for 0 kGy, 10 kGy, 20 kGy and 30 kGy, respectively. While n experiences a decrease with increasing electron dose, namely 0.39, 0.22, 0.19 and 0.11 for 0 kGy, 10 kGy, 20 kGy and 30 kGy, respectively. Thus, we observe an improvement of shear-thinning with increasing electron dose ($n < 1$ for shear-thinning of fluids). In addition, from strain sweeps, G' and G'' are visualized vs. strain, see Fig. 8. The material experiences a transition from elastic solid-like to more viscous liquid-like, referred to as the crossover point ($G' = G''$). The crossover point slightly changed after irradiation, as shown in Fig. 9. Herein, it is plotted as a function of electron dose obtained from interpolation of the γ sweeps. The crossover point experiences a reduction to lower strains from 3.26 % to 2.53 %. Thus, with increasing electron irradiation the material transitions faster into liquid-like behavior. Consequently, smaller shear strains are sufficient to disrupt the granular network connections and enable flow. This dynamic behavior might be expected for a granular material, since solid-like

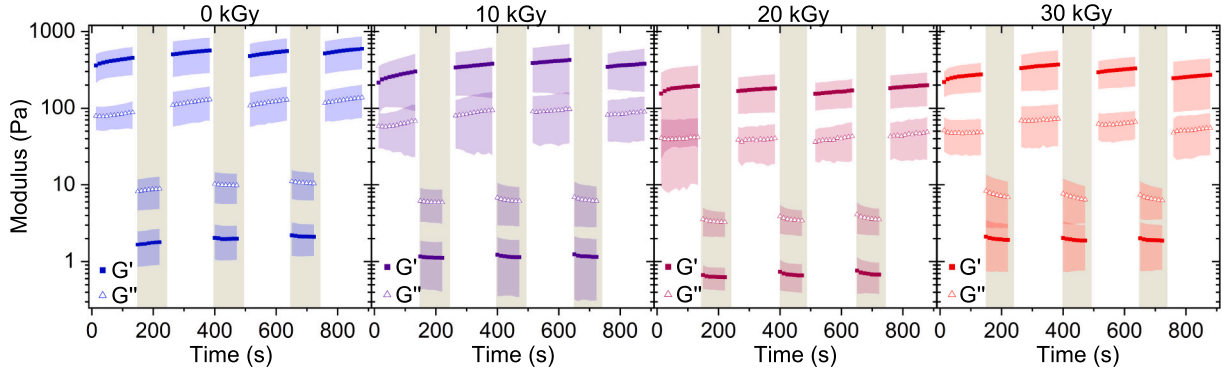

Fig. 6. Storage G' and loss modulus G'' vs. time by cycling between strains of 0.1 % (low strain) and 1000 % (high strain = grey region) at constant frequency of 1 Hz. The moduli obtained from high-strain regions are highlighted in grey.

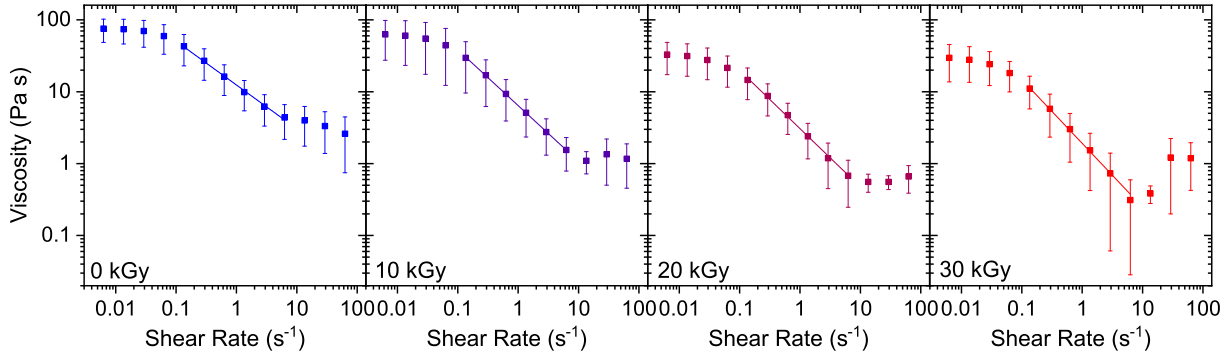

Fig. 7. Viscosity η as a function of shear rate $\dot{\gamma}$ determined from strain γ sweeps in the range 0.1 %–1000 % at a constant frequency of 1 Hz. Electron doses as indicated.

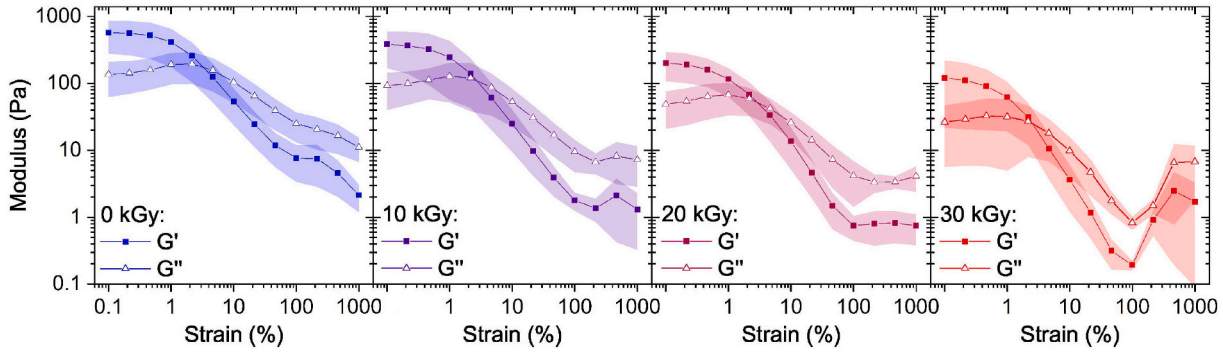

Fig. 8. Storage G' and loss modulus G'' over strain γ by rheology measurements at constant frequency of 1 Hz. Electron doses as indicated.

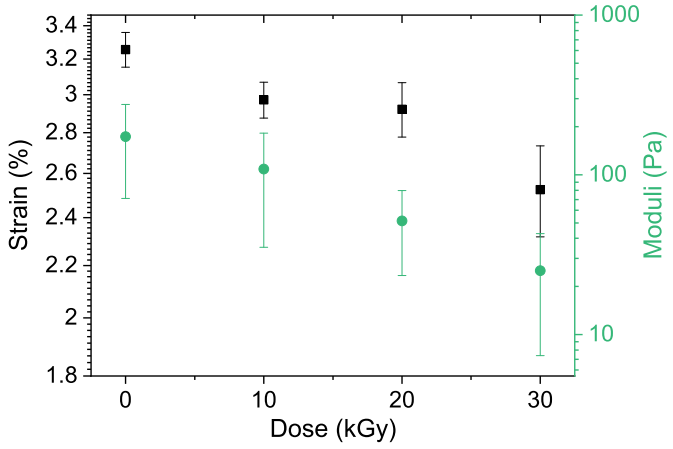

Fig. 9. Crossover point $G' = G''$ as a function of electron dose calculated by interpolation of strain γ sweeps. Error determined by propagation.

behavior results from relatively weak frictional forces between jammed beads. The slight increase of G'' before the crossover point might be attributed to the energy dissipation induced by the rearrangement of jammed beads and is in accordance with literature (Franco et al., 2021). However, although self-healing and shear-thinning is preserved within all electron doses, G' and G'' experience a degradation. In the dose range, the rheological mechanics decrease by nearly 40 %. This is assigned to radiation induced degradation of the polysaccharides. Degraded mechanics for irradiated bulk agarose and alginate are already reported and are assigned to the decreasing molecular weight and cleavage of glycosidic bonds (Wang et al., 2015; Wasikiewicz et al., 2005).

Overall, self-healing in combination with the elastic-to-viscous transition makes the material suitable for syringe injections and provides stabilization after injection. Injection is advantageous for many biomedical applications and is exemplary shown in Fig. S2 of the supplementary material, where the granular hydrogel is pressed through a 27 G needle.

3.4. AFM

Microrheology measurements on individual beads were performed by AFM employing spherical Hertz model (Hertz, 1882). Storage G' and loss moduli G'' are shown in Fig. 10. The overall degradation characterized by a decrease in mechanical stability, as observed for the whole granular hydrogel, is also visible in AFM measurements on individual beads. For 30 kGy, the viscoelasticity experience a reduction of ~50% similarly to the rheometer measurements shown before. As reported for conventional polysaccharidic hydrogels such as agarose and alginate, the mechanical degradation proceeds by breakage of glycosidic bonds (Wang et al., 2015; Wasikiewicz et al., 2005). For each electron dose, rheological properties of the single beads can roughly be described in terms of a power-law. This rheological scale-free behavior in frequency and time is also reported for living cells or soft glassy materials (Kollmannsberger & Fabry, 2011). However, within an electron dose, no trend between radius of the beads and viscoelasticity is observed (results not shown here). This could have indicated an increased pressure in spheres compared to bulk hydrogel due to surface tension effects. For all electron doses, the mechanics are significantly higher than those of the granular hydrogel. At a frequency of 1 Hz, G' of individual beads is more than an order of magnitude larger than that of the granular hydrogel. This is probably due to the available interstitial space between the beads in rheology measurements. However, discrepancies may also occur by the usage of two different measurement methods.

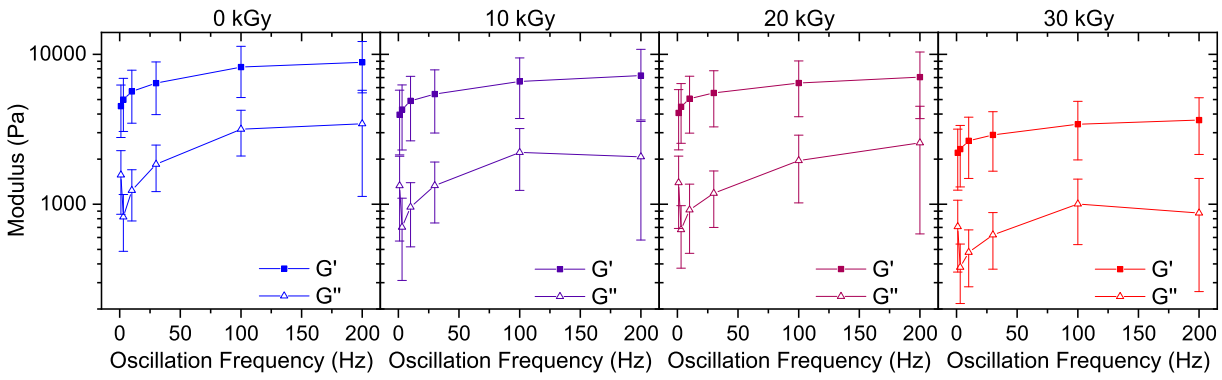

Fig. 10. Storage G' and loss moduli G'' over frequency determined from AFM measurements of 1 wt% agarose/alginate beads with different electron doses.

4. Conclusion

This study provides a mechanical characterization of injectable, electron irradiated agarose/alginate beads. The beads are prepared by electrospraying using voltages of 5 kV, 10 kV and 15 kV and a fixed flow rate. Radii analysis was performed using optical methodology based on circular Hough transformation. An increasing voltage results in smaller agarose/alginate beads on average. For all voltages, nearly constant polydispersity is observed with an index of ~0.05. Since electron irradiation is an effective and advantageous technique to sterilize biomedical products, we study its impact on the size distribution and mechanical characteristics. Therefore, we employed 10 MeV fast electrons in typical sterilization doses from 0 kGy to 30 kGy. Application of 30 kGy leads to a reduced bead size by approx. 20 %. Electron irradiation is accompanied by the formation of secreted species, which are released from the agarose/alginate beads and probably lead to the general size reduction of the agarose/alginate beads. The mechanics of the beads were characterized using two methods: rotational oscillation rheology of the granular hydrogel and microrheology of individual beads by AFM. For all electron doses, the granular hydrogel maintained shear-thinning and self-healing, examined by cycling between high and low strain regions. Functionally, shear-thinning behavior permits injectability through 27 G needles, without further chemical modification. Furthermore, mechanics are maintained after injection, indicated by its self-healing function, making it attractive for application in biomedicine. Mechanical characterization revealed a reduction of the viscoelasticity of the granular hydrogel and of individual beads due to radiolytic degradation under electron irradiation. But since overall shear-thinning and self-healing behavior is maintained up to 30 kGy, we judge agarose/alginate beads as radiation resistant enough for application. By modifying the size distribution and adjusting viscoelasticity of agarose/alginate beads, high-energy electron irradiation is demonstrated to be an effective instrument. Based on mechanical degradation of individual beads and of the granular hydrogel, the applicability is limited only at higher electron doses.

In the future, biomedical application of the presented beads needs to be assessed and usability in tissue engineering or drug delivery needs to be tested. In particular, encapsulation of a model drug and its controlled release in terms of the applied electron dose should be considered.

Supplementary data to this article can be found online at https://doi.org/10.1016/j.carbpol.2022.120024.

CRediT authorship contribution statement

Catharina Krömmelbein: Conceptualization, Methodology, Validation, Formal analysis, Investigation, Writing – original draft, Writing – review & editing, Visualization. **Xiaofan Xie:** Validation, Investigation, Writing – review & editing. **Jakob Seifert:** Software, Validation, Investigation, Writing – review & editing. **Robert Konieczny:** Resources, Writing – review & editing. **Sabrina Friebe:** Software, Writing – review & editing. **Josef Käs:** Resources, Writing – review & editing. **Stefanie Riedel:** Conceptualization, Methodology, Writing – review & editing, Supervision, Project administration, Funding acquisition. **Stefan G. Mayr:** Resources, Writing – review & editing, Supervision, Project administration, Funding acquisition.

Declaration of competing interest

We have no conflicts of interest to declare.

Data availability

Data will be made available on request.

Acknowledgments

We gratefully acknowledge Dr. Knolle (IOM Leipzig, Germany) for electron irradiation and our project partners Dr. Gerdes and Dr. Stadler (Cell.Copedia GmbH, Leipzig, Germany). This study was partially performed within the Leipzig graduate school of Natural Sciences - Building with Molecules and Nanoobjects. The research was funded by the Free State of Saxony and the European Regional Development Fund as part of the project “CC Top” (grant no.: 100362596) and the German Research Foundation (DFG), Project MA 2432/12-1.

References

Alcaraz, J., Buscemi, L., Grabulosa, M., Trepat, X., Fabry, B., Farré, R., & Navajas, D. (2003). Microrheology of human lung epithelial cells measured by atomic force microscopy. *Biophysical Journal, 84*(3), 2071–2079.

Alizadeh, R., Zarrintaj, P., Kamrava, S. K., Bagher, Z., Farhadi, M., Heidari, F., Komeili, A., Gutiérrez, T. J., & Saeb, M. R. (2019). Conductive hydrogels based on agarose/alginate/chitosan for neural disorder therapy. *Carbohydrate Polymers, 224*, Article 115161.

An, J., Kim, S., Shrinidhi, A., Kim, J., Banna, H., Sung, G., Park, K. M., & Kim, K. (2020). Purification of protein therapeutics via high-affinity supramolecular host–guest interactions. *Nature Biomedical Engineering, 4*(11), 1044–1052.

Ashfaq, A., Clochard, M. C., Coqueret, X., Dispenza, C., Driscoll, M. S., Ulański, P., & Al-Sheikhly, M. (2020). Polymerization reactions and modifications of polymers by ionizing radiation. *Polymers, 12*(12), 2877.

Aswathy, S. H., Narendrakumar, U., & Manjubala, I. (2020). Commercial hydrogels for biomedical applications. *Heliyon, 6*(4), Article e03719.

Chen, R., Shi, J., Liu, C., Li, J., & Cao, S. (2021). In situ self-assembly of gold nanorods with thermal-responsive microgel for multi-synergistic remote drug delivery. *Advanced Composites and Hybrid Materials, 1*, 1–12.

Chen, X. Y., Chen, J. Y., Tong, X. M., Mei, J. G., Chen, Y. F., & Mou, X. Z. (2020). Recent advances in the use of microcarriers for cell cultures and their ex vivo and in vivo applications. *Biotechnology Letters, 42*(1), 1–10.

Cheng, W., Zhang, J., Liu, J., & Yu, Z. (2020). Granular hydrogels for 3D bioprinting applications. *View, 1*(3), Article 20200060.

Daly, A. C., Riley, L., Segura, T., & Burdick, J. A. (2019). Hydrogel microparticles for biomedical applications. *Nature Reviews Materials, 5*(1), 20–43.

De France, K. J., Xu, F., & Hoare, T. (2018). Structured macroporous hydrogels: Progress, challenges, and opportunities. *Advanced Healthcare Materials, 7*(1), 1700927.

de la Mora, J. F., & Loscertales, I. G. (1994). The current emitted by highly conducting Taylor cones. *Journal of Fluid Mechanics, 260*, 155–184.
Franco, S., Buratti, E., Nigro, V., Zaccarelli, E., Ruzicka, B., & Angelini, R. (2021). Glass and jamming rheology in soft particles made of pnipam and polyacrylic acid. *International Journal of Molecular Sciences, 22*(8), 4032.
Gilbert, D., Valette, R., & Lemaire, E. (2022). Impact of particle stiffness on shear-thinning of non-Brownian suspensions. *Journal of Rheology, 66*(1), 161–176.
Guastaferro, M., Reverchon, E., & Baldino, L. (2021). Agarose, alginate and chitosan nanostructured aerogels for pharmaceutical applications: A short review. *Frontiers in Bioengineering and Biotechnology, 9*.
Hartman, R. P., Brunner, D. J., Camelot, D. M., Marijnissen, J. C., & Scarlett, B. (2000). Jet break-up in electrohydrodynamic atomization in the cone-jet mode. *Journal of Aerosol Science, 31*(1), 65–95.
He, H., Wu, M., Zhu, J., Yang, Y., Ge, R., & Yu, D.-G. (2022). Engineered spindles of little molecules around electrospun nanofibers for biphasic drug release. *Advanced Fiber Materials, 4*(2), 305–317.
Hennink, W. E., & van Nostrum, C. F. (2012). Novel crosslinking methods to design hydrogels. *Advanced Drug Delivery Reviews, 64*, 223–236.
Hertz, H. (1882). Ueber die Berührung fester elastischer Körper. *Journal fur die Reine und Angewandte Mathematik, 92*, 156–171.
Hough, P. V. C. (1962). *Method and means for recognizing complex patterns. US Patent No. 3,069,654*.
Ighigeanu, D., Martin, D., Manaila, E., Stan, D. E., Baciu, I. V., Craciun, G., & Oproiu, C. (2006). Electron Beam Sterilization of the Agarose Gel Used for Electrophoresis. In *Utilization of accelerators, Proceedings of an international conference*.
Jafari-Nodoushan, M., Barzin, J., & Mobedi, H. (2015). Size and morphology controlling of PLGA microparticles produced by electro hydrodynamic atomization. *Polymers for Advanced Technologies, 26*(5), 502–513.
Jeon, O., Lee, Y. B., Jeong, H., Lee, S. J., Wells, D., & Alsberg, E. (2019). Individual cell-only bioink and photocurable supporting medium for 3D printing and generation of engineered tissues with complex geometries. *Materials Horizons, 6*(8), 1625–1631.
Khodadadi Yazdi, M., Taghizadeh, A., Taghizadeh, M., Stadler, F. J., Farokhi, M., Mottaghitalab, F., Zarrintaj, P., Ramsey, J. D., Seidi, F., Saeb, M. R., & Mozafari, M. (2020). Agarose-based biomaterials for advanced drug delivery. *Journal of Controlled Release, 326*, 523–543.
Kim, J., Hiltpold, I., Jaffuel, G., Sbaiti, I., Hibbard, B. E., & Turlings, T. C. (2021). Calcium-alginate beads as a formulation for the application of entomopathogenic nematodes to control rootworms. *Journal of Pest Science, 94*(4), 1197–1208.
Kollmannsberger, P., & Fabry, B. (2011). Linear and nonlinear rheology of living cells. *Annual Review of Materials Research, 41*, 75–97.
Krömmelbein, C., Mütze, M., Konieczny, R., Schönherr, N., Griebel, J., Gerdes, W., Mayr, S. G., & Riedel, S. (2021). Impact of high-energy electron irradiation on mechanical, structural and chemical properties of agarose hydrogels. *Carbohydrate Polymers, 263*(117970).
Landau, L. D., & Lifshitz, E. M. (1959). *Theory of Elasticity*. Cambridge University Press.
Li, D., Wang, M., Song, W.-L., Yu, D.-G., & Bligh, S. W. A. (2021). Electrospun janus beads-on-A-string structures for different types of controlled release profiles of double drugs. *Biomolecules, 11*(5), 635.
Liu, Z., Chen, H., Lv, F., Wang, J., Zhao, S., Li, Y., Xue, X., Liu, Y., Wei, G., & Lu, W. (2021). Sequential release of paclitaxel and Imatinib from Core-Shell microparticles prepared by coaxial electrospray for vaginal therapy of cervical cancer. *International Journal of Molecular Sciences, 22*(16), 8760.
Mahaffy, R. E., Shih, C. K., MacKintosh, F. C., & Käs, J. (2000). Scanning probe-based frequency-dependent microrheology of polymer gels and biological cells. *Physical Review Letters, 85*(4), 880.
Moxon, S. R., Cooke, M. E., Cox, S. C., Snow, M., Jeys, L., Jones, S. W., Smith, A. M., & Grover, L. M. (2017). Suspended manufacture of biological structures. *Advanced Materials, 29*(13), 1605594.
Muir, V. G., Qazi, T. H., Shan, J., Groll, J., & Burdick, J. A. (2021). Influence of microgel fabrication technique on granular hydrogel properties. *ACS Biomaterials Science and Engineering, 7*(9), 4269–4281.
Nagasawa, N., Mitomo, H., Yoshii, F., & Kume, T. (2000). Radiation-induced degradation of sodium alginate. *Polymer Degradation and Stability, 69*(3), 279–285.
Orive, G., Hernández, R. M., Gascón, A. R., Igartua, M., Rojas, A., & Pedraz, J. L. (2001). Microencapsulation of an anti-VE–cadherin antibody secreting 1B5 hybridoma cells. *Biotechnology and Bioengineering, 76*(4), 285–294.
Ostwald, W. (1925). Ueber die geschwindigkeitsfunktion der Viskosität disperser systeme. *I. Kolloid-Zeitschrift, 36*(2), 99–117.
Park, H., Kim, P. H., Hwang, T., Kwon, O. J., Park, T. J., Choi, S. W., Yun, C. O., & Kim, J. H. (2012). Fabrication of cross-linked alginate beads using electrospraying for adenovirus delivery. *International Journal of Pharmaceutics, 427*(2), 417–425.
Qazi, T. H., & Burdick, J. A. (2021). Granular hydrogels for endogenous tissue repair. *Biomaterials and Biosystems, 1*, Article 100008.
Riley, L., Schirmer, L., & Segura, T. (2019). Granular hydrogels: Emergent properties of jammed hydrogel microparticles and their applications in tissue repair and regeneration. *Current Opinion in Biotechnology, 60*, 1–8.
Rosell-Llompart, J., & Fernández de la Mora, J. (1994). Generation of monodisperse droplets 0.3 to 4 m in diameter from electrified cone-jets of highly conducting and viscous liquids. *Journal of Aerosol Science, 25*(6), 1093–1119.
Schneider, C. A., Rasband, W. S., & Eliceiri, K. W. (2012). NIH image to ImageJ: 25 years of image analysis. *Nature Methods, 9*(7), 671–675.
Vicini, S., Castellano, M., Mauri, M., & Marsano, E. (2015). Gelling process for sodium alginate: New technical approach by using calcium rich micro-spheres. *Carbohydrate Polymers, 134*, 767–774.
von Sonntag, C. (1980). Free-radical reactions of carbohydrates as studied by radiation techniques. *Advances in Carbohydrate Chemistry and Biochemistry, 37*, 7–77.
Wang, X., Ao, Y.-Y., Huang, W., Liu, B., An, Y., & Zhai, M.-L. (2015). Radiation effects on physically cross-linked agarose hydrogels. *Nuclear Science and Techniques, 26*(5), Article 050304.
Wasikiewicz, J. M., Yoshii, F., Nagasawa, N., Wach, R. A., & Mitomo, H. (2005). Degradation of chitosan and sodium alginate by gamma radiation, sonochemical and ultraviolet methods. *Radiation Physics and Chemistry, 73*(5), 287–295.
Wisotzki, E. I., Hennes, M., Schuldt, C., Engert, F., Knolle, W., Decker, U., Käs, J. A., Zink, M., & Mayr, S. G. (2014). Tailoring the material properties of gelatin hydrogels by high energy electron irradiation. *Journal of Materials Chemistry B, 2*(27), 4297–4309.
Wu, Y. Q., & Clark, R. L. (2007). Controllable porous polymer particles generated by electrospraying. *Journal of Colloid and Interface Science, 310*(2), 529–535.
Zakeri, M., Moghadam, H., Samimi, A., & Mohebbi-Kalhori, D. (2019). Optimization of calcium alginate beads production by electrospray using response surface methodology. *Materials Research Express, 6*(9), Article 095412.
Zeng, Q., Han, Y., Li, H., & Chang, J. (2015). Design of a thermosensitive bioglass/agarose–alginate composite hydrogel for chronic wound healing. *Journal of Materials Chemistry B, 3*(45), 8856–8864.